Effect of Wire Preheat and Feed Rate in X80 Steel Laser Root Welds: Part 2 — Mechanical Properties

A hot-wire feed can reduce weld metal hardness and improve the toughness of X80 laser welds

BY H. YANG, J. CHEN, N. HUDA, X. ZHAO, AND A.P. GERLICH

Abstract

In Part 1 of this study, the influences of feed rate and preheat of the wire on the fusion zone microstructure of X80 steel laser root welds were investigated. Part 2 of this study reveals the effect of cold versus hot wire feed on mechanical properties. Although strength overmatching with the X80 base metal was maintained, the wire alloying elements reduced the hardness of the upper region of the laser fusion zone but had limited effect on the bottom of the fusion zone due to the incomplete mixing of the filler material with the base metal in the bottom root region of the joint. The addition of ER70S-6 filler wire improved the impact toughness of the weld metal at 0°C, due to the formation of an acicular ferrite microstructure. As the temperature decreased to –20°C (–4°F) and –45°C (–49°F), ductile to brittle transition occurred, leading to lower weld metal toughness.

Keywords

- Hot-Wire Laser Welding
- Acicular Ferrite
- Microhardness
- Charpy Impact Toughness
- Ductile to Brittle Transition

Introduction

Morden pipelines are made of high-strength low alloy (HSLA) steels due to their high strength and superior toughness (Ref. 1). Welding is an essential process for fabricating large-scale pipelines, which determines the productivity and reliability of the pipeline system. Replacing conventional welding methods like submerged arc welding (SAW) and gas metal arc welding (GMAW) with laser or hybrid laser welding can significantly increase productivity and may reduce construction costs through a combination of high welding speed and deep penetration (Ref. 1). However, for the welding of carbon steels, autogenous laser welding has drawbacks including poor gap-bridging ability (Refs. 2–4), and a high cooling rate which could result in the weld metal brittleness (Refs. 1, 5). In recent years, novel technologies like hybrid laser arc welding (HLAW) (Refs. 6, 7) and hot-wire laser welding (HWLW) (Refs. 5, 8, 9) have been developed to improve the welding performance. Feeding an additional wire could increase the gap tolerance (Ref. 8) and modify the chemical composition and weld metal microstructure (Ref. 5). Phillips et al. (Ref. 5) found that hot-wire feed during laser welding of HY80 and HY100 steel reduced the weld metal hardness while also increasing the Charpy V-notch toughness by promoting the formation of acicular ferrite instead of martensite in the fusion zone. Metzbower et al. (Ref. 10) reported that during laser welding of HY80 steel, a hot-wire feed led to a lower cooling rate in the molten pool and hence limited the formation of martensite. They found that compared to an untempered martensite structure obtained in the autogenous weld, a mixed martensite-bainite microstructure was obtained with a slow hot-wire feed, and a primarily acicular ferrite microstructure was achieved with a fast feed, which led to the lower hardness of the weld metal.

In Part 1 of this study, the influences of filler material volume and wire preheat on the weld metal microstructure during laser welding of X80 steel were investigated. The microstructure evolution in heat affected zone (HAZ) was also discussed. The results showed that increasing the wire feed rate helped generate acicular ferrite in the weld metal by modifying the chemical composition, and preheating the wire further suppressed the formation of bainite. The uneven distribution of the filler material resulted in a difference in fusion zone microstructure along the thickness direction.
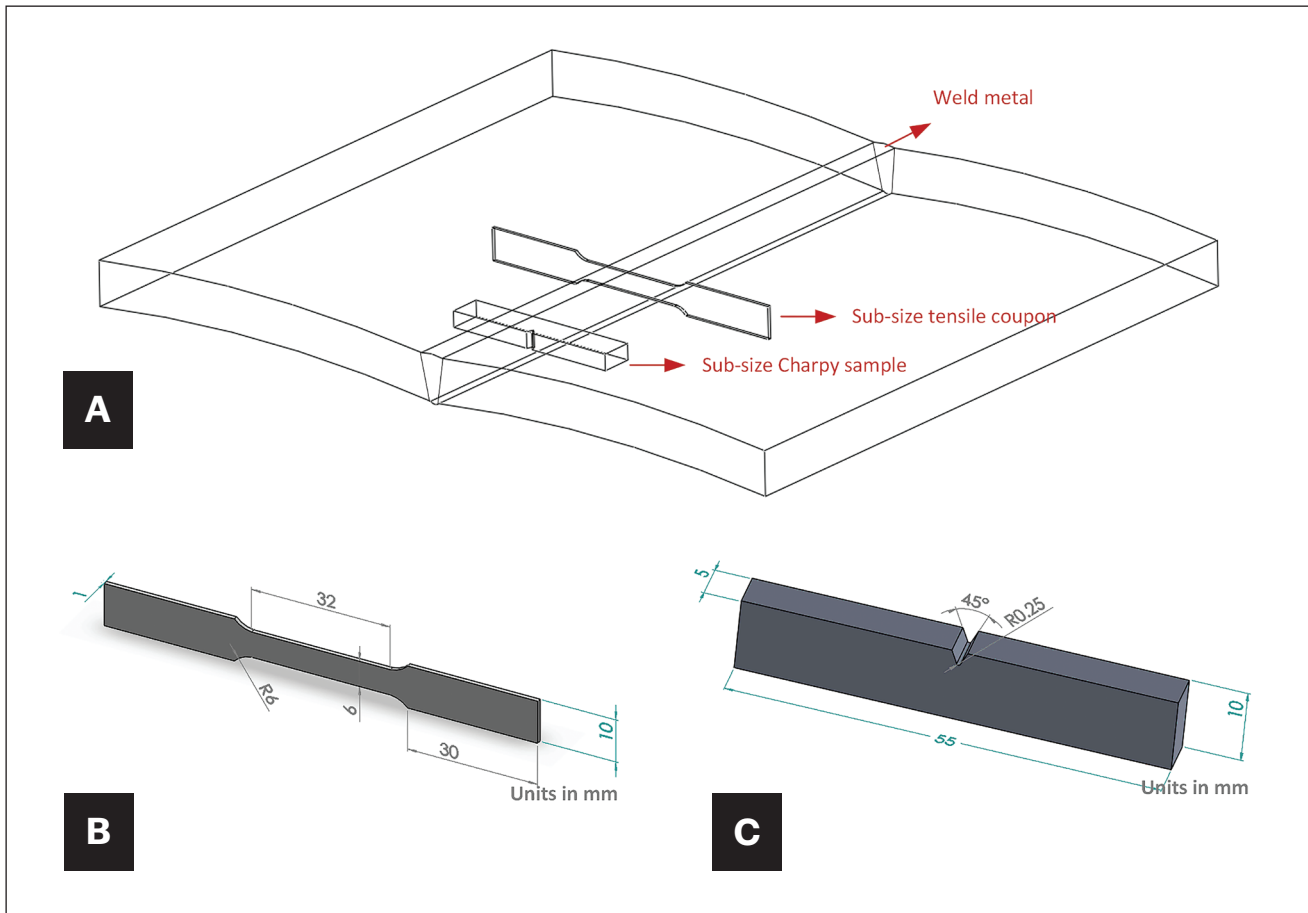
Fig. 1 — A — Schematic diagram showing the extraction position of tensile and Charpy samples; B — dimensions of sub-size tensile coupon; C — dimensions of sub-size Charpy sample.

In this second part of the work, the effect of wire feed rate (WFR) and preheat of the wire on the mechanical properties, including hardness, tensile strength, and Charpy V-notch impact toughness, are investigated. The process-microstructure-properties relationship is also discussed in the context of microstructures discussed in the first part of the study.

Experimental Procedures

Welding Test Design

A brief reintroduction of the welding experimental work is given here. Further details can be found in Part 1 of this study (Ref. 11). Wire-fed laser welding with a 0.9 mm (0.035 in.) ER70S-6 wire was performed on 14-mm-thick X80 steel plates, with a groove having a 6 mm root height and a 30-degree included angle. Five passes of GMAW welds with the same welding wire were then applied to fill the top part of the groove (with a WFR of 6.9 m/min, a travel speed of 0.13 m (0.005 in.)/min, a welding current of around 143.7 A and a welding voltage of 19 V). Four of the laser welds were chosen to compare mechanical properties, with the welding parameters listed in Table 1.

Microstructure and Mechanical Properties Analysis

The cross-sectional samples were cut out and polished for microhardness tests and microstructural analysis. The samples were etched with Nital, a mixture of 5% nitric acid and 95% ethanol, for 5 s to reveal the microstructure based on ASTM E407. The Vickers microhardness was measured in the laser root weld using a Clemex instrumented indentation microhardness tester, with a load of 500 g (1.102 lb) and a dwell time of 10 s. The hardness map covered half of the joint from the weld centerline to the base metal, with a 200 $\mu m \times 250 \mu m$ step size. The average values of 5 indentation lines from the weld top surface were calculated for hardness distribution analysis, and the mean weld metal hardness was then calculated by averaging the hardness of indents located in the fusion zone, with a 95% confidence interval for statistical analysis. The weld metal hardness distribution along the through-thickness direction was also analyzed by averaging the hardness values of 4 indentation lines located in the fusion zone. After the microhardness test, an Olympus BX51 optical microscope (OM) was utilized to identify the indentation locations and characterize the microstructure.
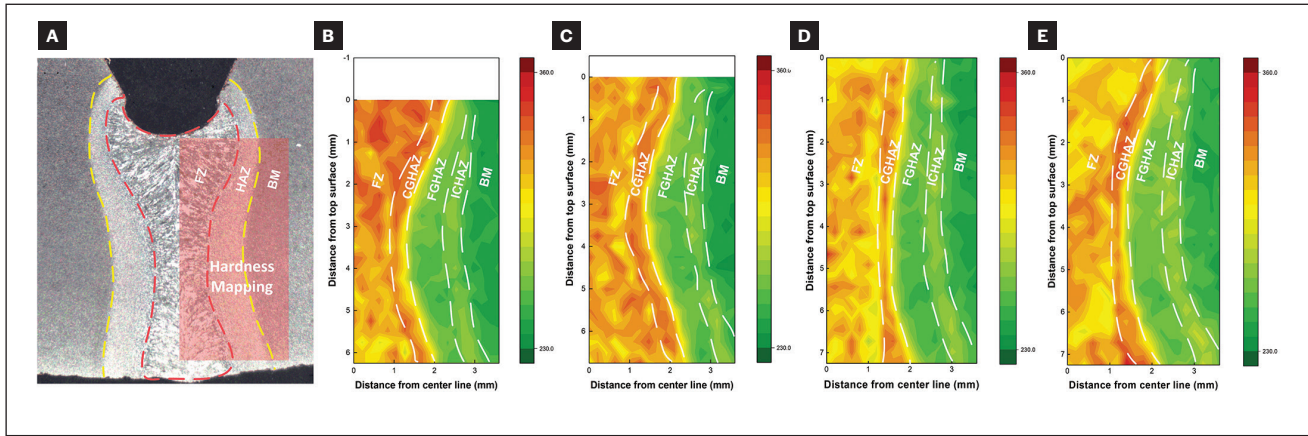
Fig. 2 — A — Macrograph showing the hardness mapping location; B — hardness mapping results of autogenous laser weld; C — hardness mapping results of cold-wire laser weld with a WFR of 6 m/min; D — hardness mapping results of cold-wire laser weld with a WFR of 12 m/min; E — hardness mapping results of hot-wire laser weld with a WFR of 12 m/min.

Table 1 — Welding Parameters of the Welds Selected for Mechanical Properties Tests

Sample	Laser Power P (kW)	Welding Speed v (m/min)	Wire Feed Rate WFR (m/min)	Hot Wire Pre-heat Power P_{wire} (kW)	Root Opening d (mm)	Defocused Distance D_f (mm)
a	8	1	—	—	0	-3
b	8	1	6	—	0.4	-3
c	8	1	12	—	0.4	-3
d	8	1	12	0.5	0.4	-3

Sub-size tensile samples (according to ASTM E8) were extracted from the welded plates, with the extraction position and sample dimensions shown in Figs. 1A and 1B, respectively. The sample contained both arc and laser weld metal since the gauge width was 6 mm from the mid-thickness of the pipe wall. At least three repeat tensile tests were performed for each set of parameters, using a Tinius Olsen tensile tester and loaded at a 1 mm/min crosshead movement. The stress-strain curves are based on the sample best presenting the average tensile strength and elongation, and the average ultimate tensile strength is reported with a 95% confidence interval. The Digital Image Correlation (DIC) technique was also employed using Correlated Solutions VIC-3D software to monitor the fracture behavior and measure the strain values during the tensile tests. The localized strain was automatically calculated by the DIC software with a step size of 29 pixels and a subsize of 7 pixels. The tensile properties of X80 base metal were tested with the same coupon dimensions and testing procedure, which had a 0.2% offset yield strength of 619 ± 18 MPa and met the standard of API 5L (minimum of 80 ksi or 555 MPa).

Sub-size Charpy samples with a thickness of 5 mm (according to ASTM E23) and the notch position in the weld metal were extracted from the root laser welds, with the extraction position and sample dimensions illustrated in Figs. 1A and 1C. Charpy impact tests were performed using a Zwick pendulum instrumented impact tester at three temperatures of 0°C, –20°C (–4°F), and –45°C (–49°F), as indicated in CSA Z662. Three repeat Charpy tests were done for each set of parameters at each temperature, and the force-displacement curves were plotted based on the samples with the results close to the mean. The average Charpy impact toughness values were calculated, and the toughness-temperature curves were plotted with a 95% confidence interval presented as the error bars. SEM examination was conducted using a Zeiss Ultra SEM close to the notch area and the middle area of the Charpy fracture surfaces. Energy dispersive X-ray spectroscopy (EDX) was also utilized to analyze the chemical composition of the inclusions found on the fracture surface, with an acceleration voltage of 20 kV and a collection time of 100 s.
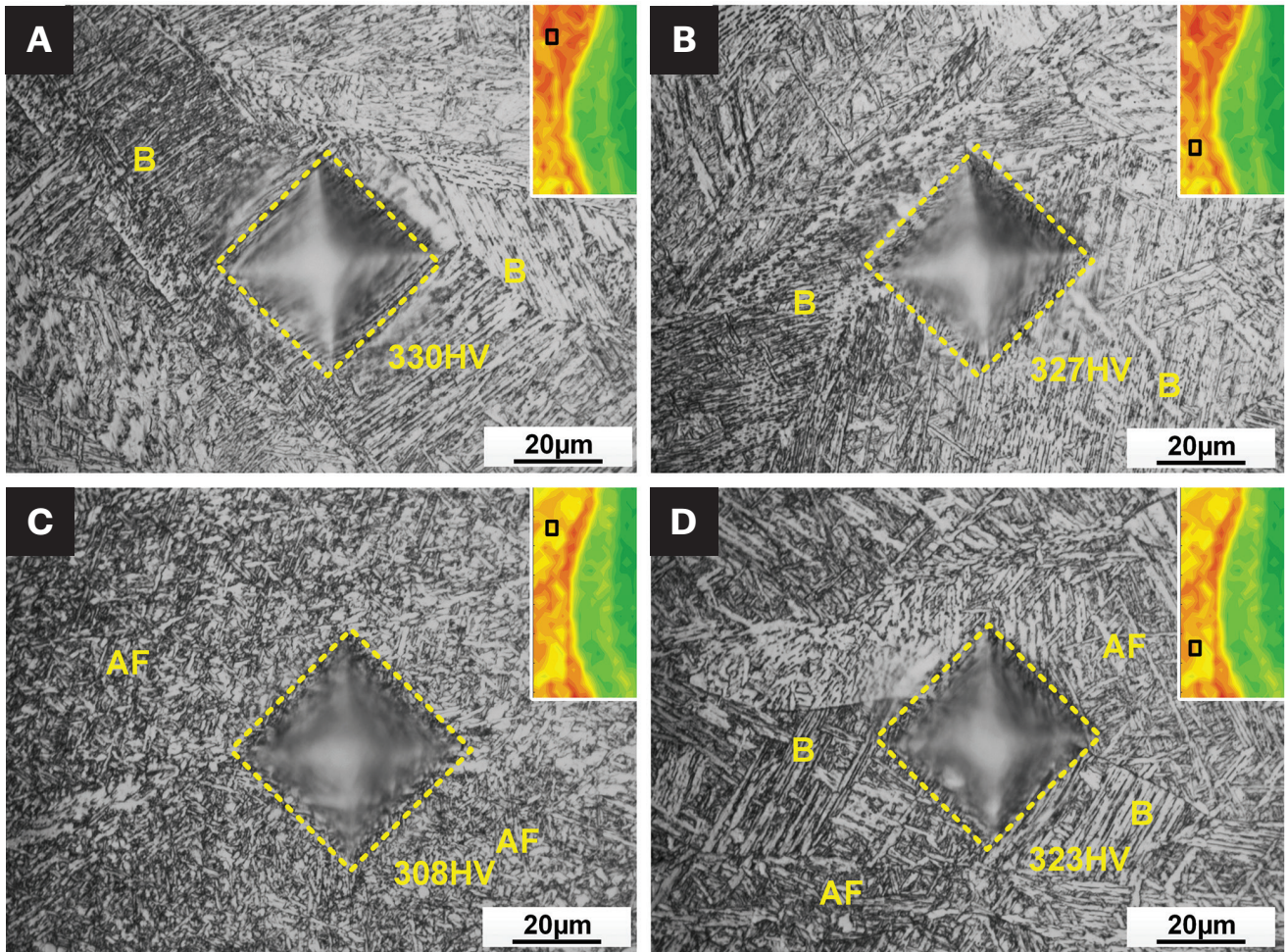
Fig. 3 — Optical micrographs showing the microhardness indentation and microstructure in: A — Upper region of the FZ in autogenous laser weld; B — lower region of the FZ in autogenous laser weld; C — upper region of the FZ in hot-wire laser weld with a WFR of 12 m/min; D — lower region of the FZ in hot-wire laser weld with a WFR of 12 m/min.
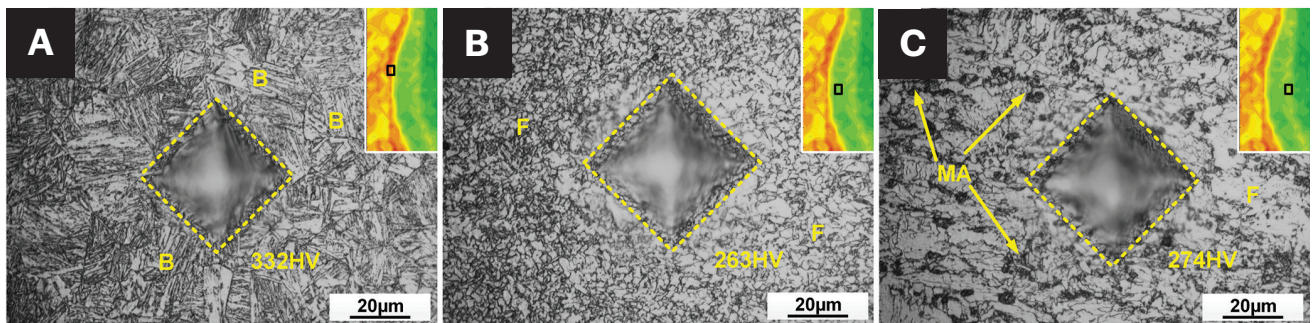
Fig. 4 — Optical micrographs showing the microhardness indentation and microstructure in the HAZ of hot-wire laser weld with a WFR of 12 m/min: A — CGHAZ; B — FGHAZ; C — ICHAZ.
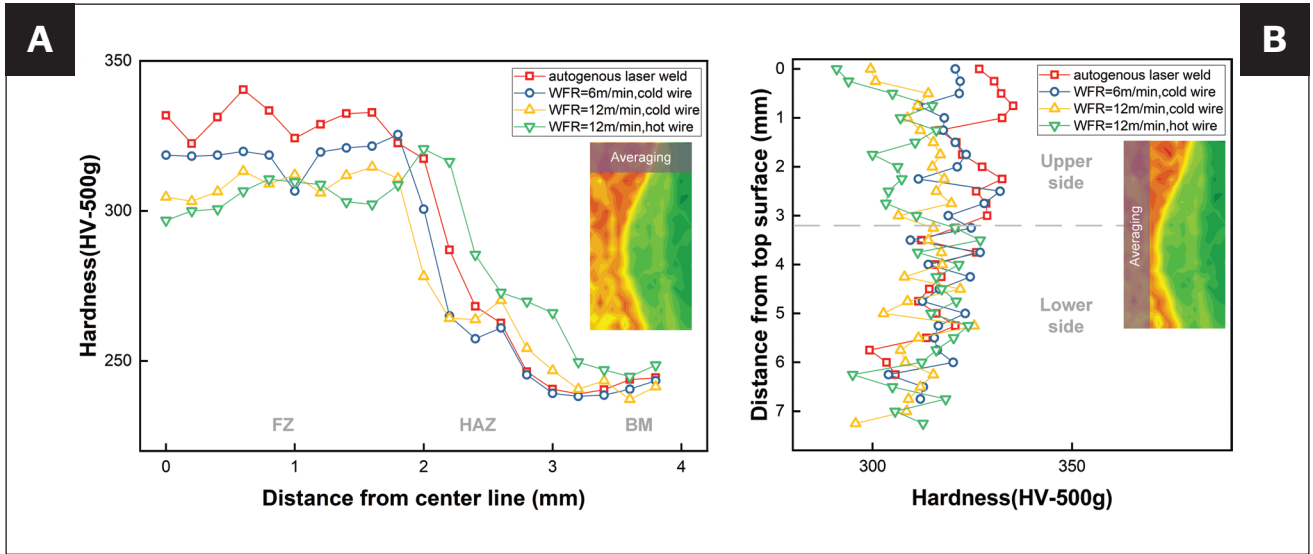
Fig. 5 — A— Top side hardness distribution of the laser root weld; B — weld metal hardness distribution of the laser root weld along the through-thickness direction.
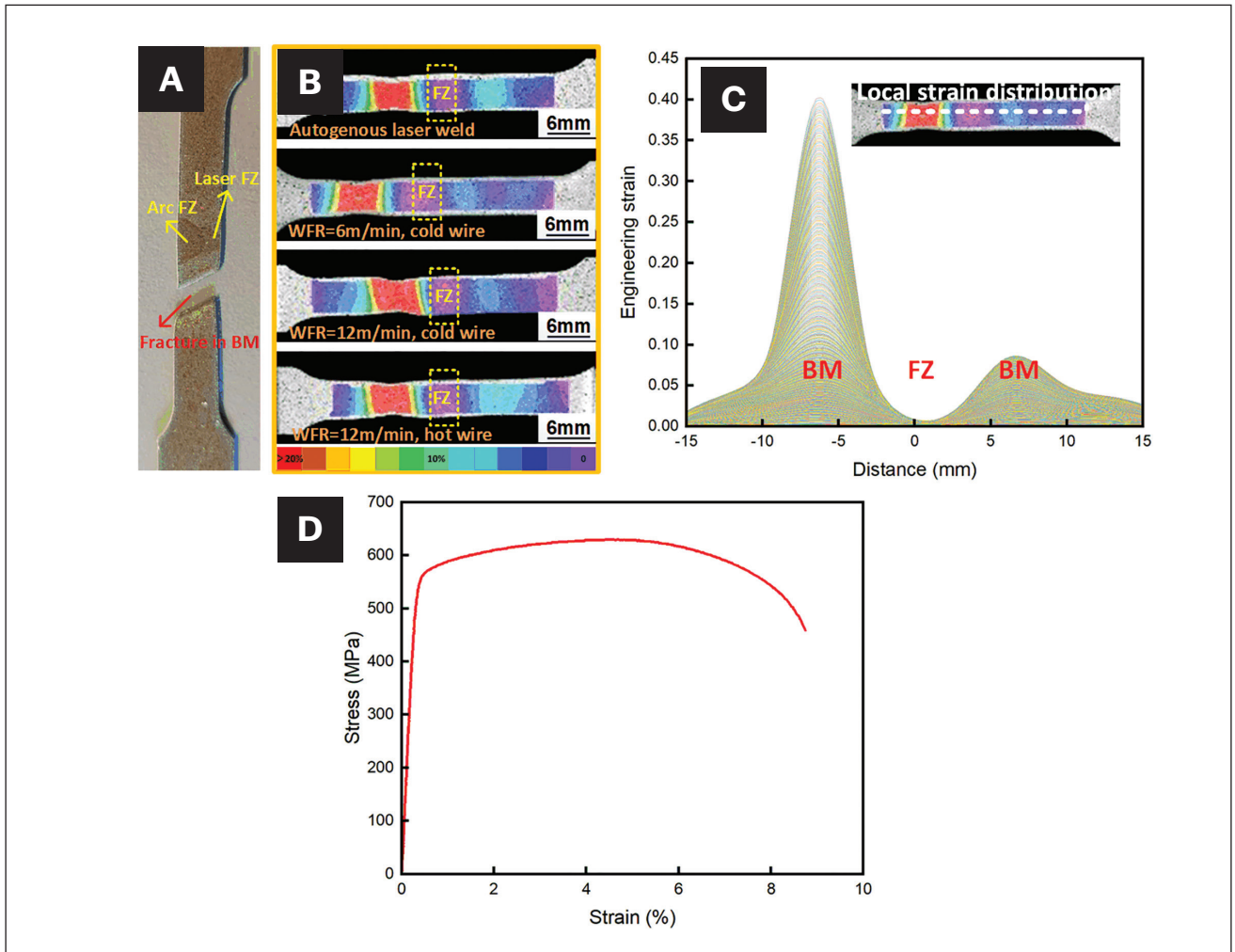
Fig. 6 — A — Tensile coupon of cold-wire laser weld with a WFR of 6 m/min, showing the fracture in the base metal; B — DIC strain maps with different welding parameters; C — local strain distribution of cold-wire laser weld with a WFR of 6 m/min; D — stress-strain curve of cold-wire laser weld with a WFR of 6 m/min.

Results and Discussion

Microhardness

Figure 2 shows the microhardness maps of the laser welded joints produced with different parameters, and the microstructure of the indentation locations in FZ and HAZ are presented in Figs. 3 and 4, respectively. The autogenous laser weld exhibited a higher FZ hardness resulting from the bainitic microstructure formed by a high cooling rate during laser welding (as shown in Fig. 3A), compared to the welds with more acicular ferrite (Fig. 3C) produced with the addition of filler material. The CGHAZ adjacent to the FZ which experienced a high peak temperature mainly contained bainite (Fig. 4A) and presented a hardness comparable to that of the FZ. A hardness peak was also found in the ICHAZ with a higher hardness than that of the FGHAZ and base metal, due to the presence of MA in this region, as shown in Fig. 4C. Figure 5A provides a more direct comparison of the hardness distribution in the upper region of the joints, meanwhile, Fig. 5B shows the FZ hardness distribution along the thickness direction. The mean hardness of the upper region of FZ in the autogenous laser weld, cold-wire laser weld with a WFR of 6 and 12 m (19.685 and 39.370 ft)/min, along with the hot-wire laser weld with a WFR of 12 m/min were averaged to be 331 ± 4, 318 ± 3, 309 ± 3 and 305 ± 4 HV, respectively. Figure 5B also clearly demonstrates the difference in the hardness of the upper region of the FZ. The upper region of the FZ in the autogenous laser weld exhibited the highest hardness, and that in the hot-wire laser weld with the high WFR of 12 m/min exhibited the lowest FZ hardness. The reduced hardness observed in the upper region of the FZ in hot-wire weld with high WFR is attributed to the decreased bainite content, as shown in Fig. 3C. However, the wire addition had no significant influence on the hardness of the lower region of the FZ, which was due to reduced filler material reaching the root region and less effect on the microstructure (as presented in Fig. 3B and D), compared to the upper region of the FZ.

API 5L indicates that the hardness of weld metal should not exceed 275 HV. The laser welds in this work exhibit higher hardness. The preheating of the plates can be done to help reduce the hardness, which is a very common strategy in industrial pipeline welding applications. However, since the motivation of this work is to investigate the effect of different heat inputs during laser welding, it would give a clearer comparison without preheating the plates.

Tensile Behavior

Due to the limited total thickness of the plates, only sub-size tensile coupons could be extracted from the welded joints, which contained both laser and arc weld metal, as
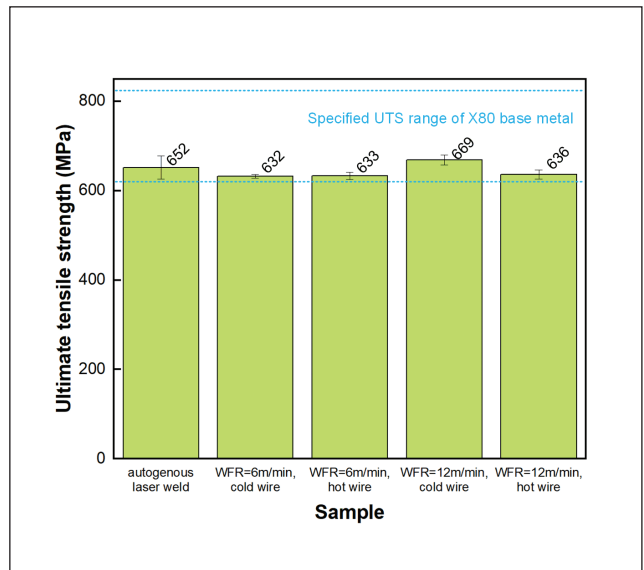
Fig. 7 — Ultimate tensile strength obtained from the transverse tensile tests.
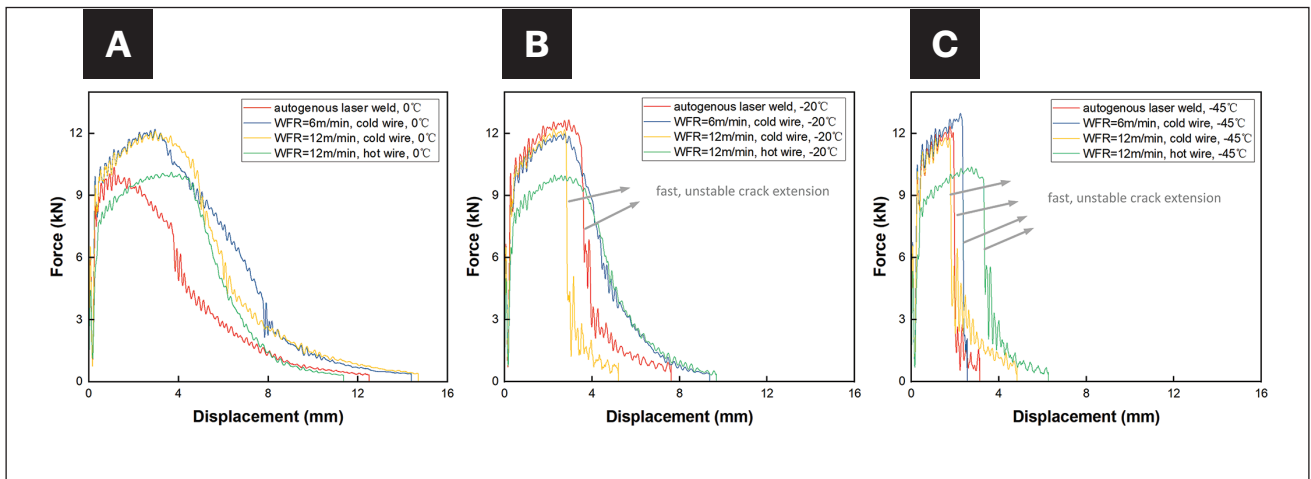
Fig. 8 — Force-displacement curves of Charpy samples at different testing temperatures: A — 0°C; B — –20°C; C — –45°C.
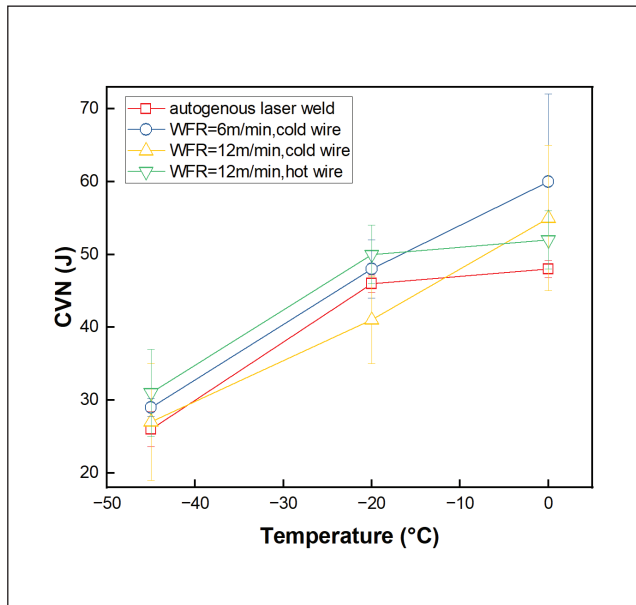
Fig. 9 — Charpy impact toughness of weld metal at different temperatures.

shown in Fig. 6A. DIC strain mapping was utilized to monitor the fracture location and local strain distribution. Figure 6B demonstrates the local strain mapping at a moment after necking happened but before the final failure. Despite the varying welding parameters, fracture occurred in the base metal for all specimens, which indicated that weld metal strength overmatch was achieved. Bainite and acicular ferrite generated in the weld metal provided a strength higher than that of the base metal. The local strain distribution shown in Fig. 6C also confirmed that the strain in the FZ was limited during the tensile test, due to the overmatching of the weld metal. The stress-strain curve of the transverse joint section is shown in Fig. 6D, and the ultimate tensile strength is reported in Fig. 7, respectively. Since the samples experienced fracture in the base metal material, the ultimate tensile strength reached was comparable and met the requirement for X80 steel listed in API 5L (625 to 825 MPa).
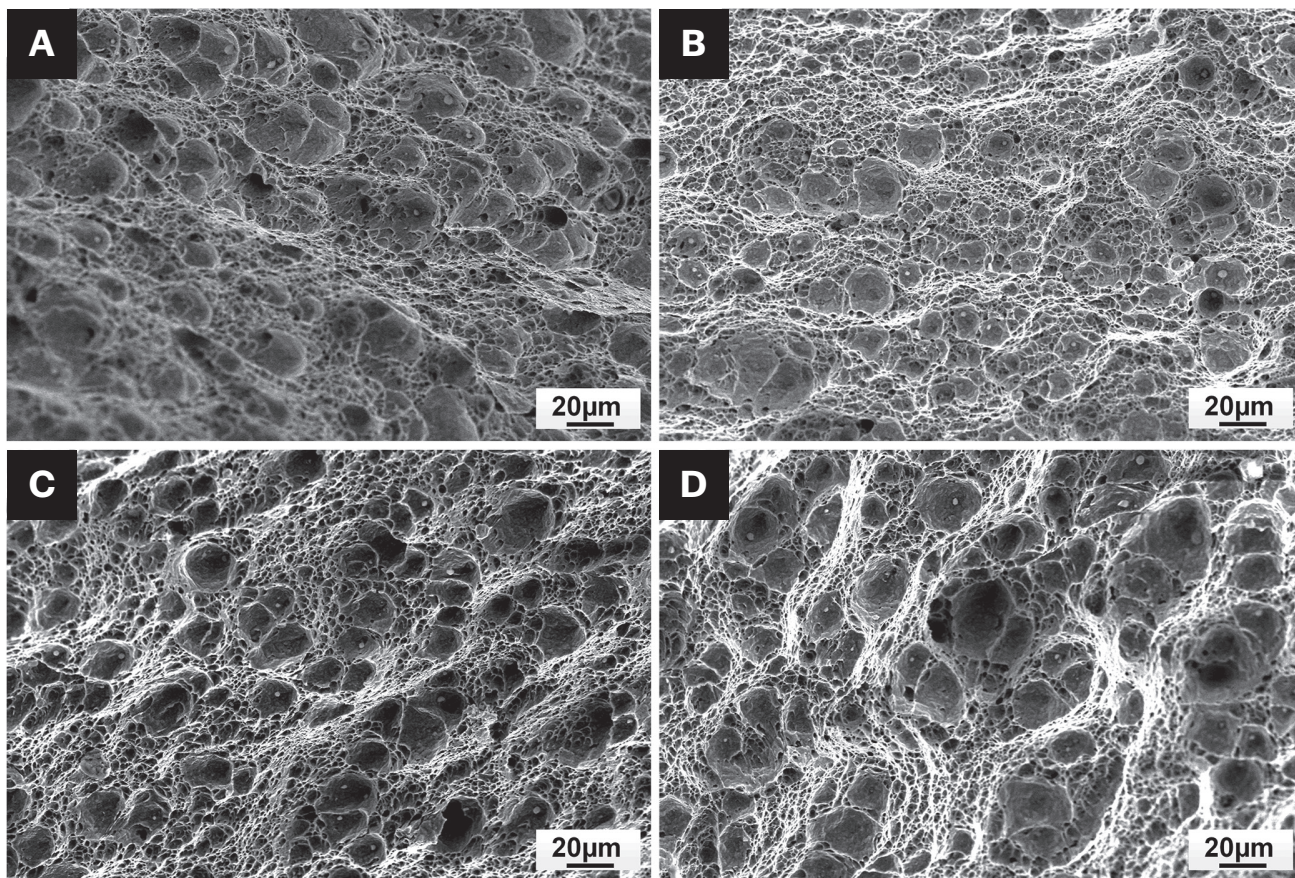
Fig. 10 — SEM images of Charpy fracture surfaces of samples tested at 0°C: A — Autogenous laser weld, near the notch; B — autogenous laser weld, toward the middle; C — cold-wire laser weld with a WFR of 12 m/min, near the notch; D — cold-wire laser weld with a WFR of 12 m/min, toward the middle.
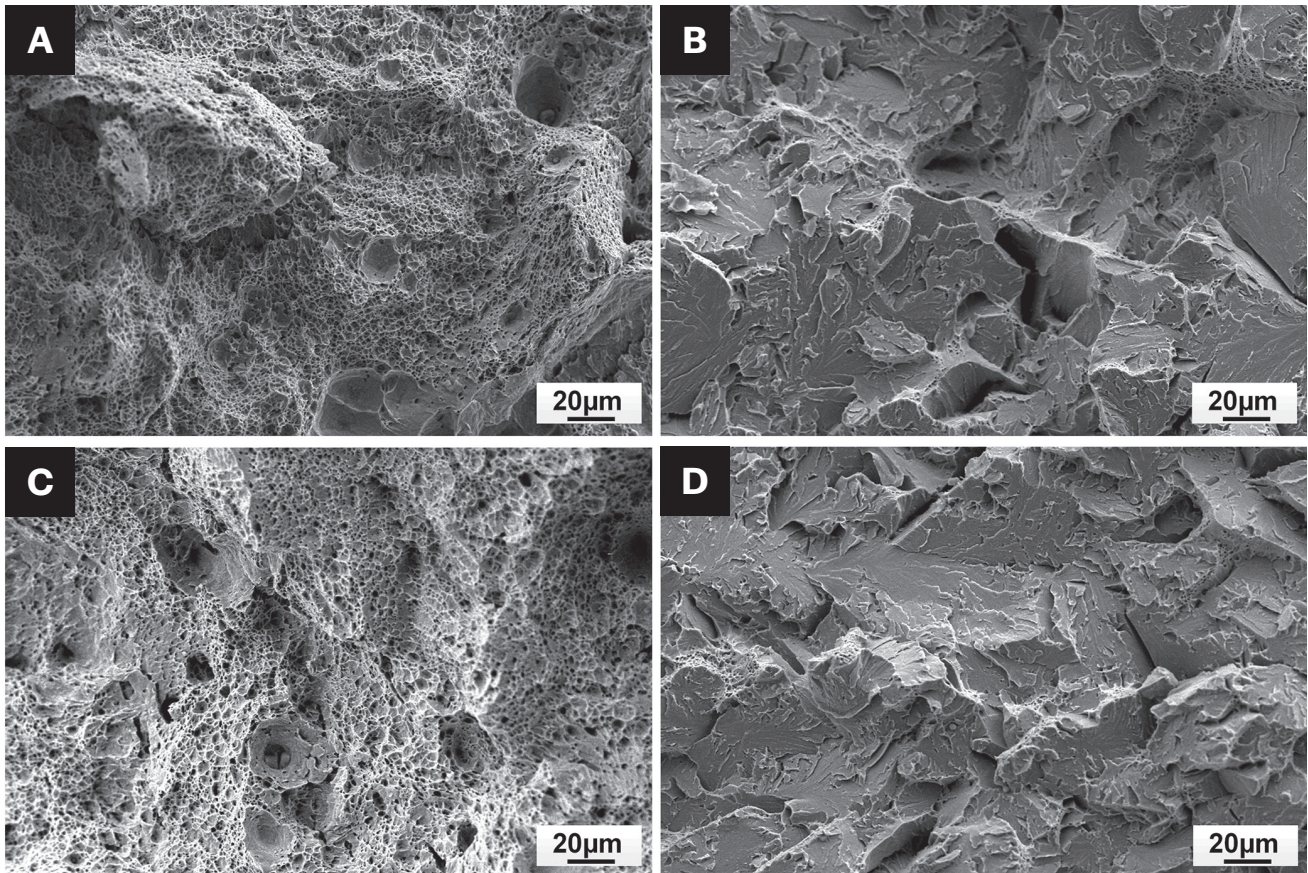
Fig. 11 — SEM images of Charpy fracture surfaces of samples tested at −20°C: A — Autogenous laser weld, near the notch; B — autogenous laser weld, towards the middle; C — cold-wire laser weld with a WFR of 12 m/min, near the notch; D — cold-wire laser weld with a WFR of 12 m/min, toward the middle.

Charpy Impact Toughness and Fracture Surfaces

Figures 8 and 9 show the force-displacement curves and impact toughness values of laser weld metal at varying Charpy testing temperatures, respectively. The ductile shear fracture occurred at 0°C, which can be derived from the force-displacement curves shown in Fig. 8A, based on the classification by ASTM E23. The trend shown in Fig. 9 indicates that the wire addition could increase the upper shelf toughness of the weld metal, where up to a 26% increase in Charpy impact toughness is achieved at the testing temperature of 0°C by feeding wire with a WFR of 6 to 12 m/min. The presence of acicular ferrite with an interlocking structure formed by wire addition accounts for the improved crack arrest ability of the weld metal, leading to an increase in impact toughness. As the temperature decreased to −20°C and −45°C, fast and unstable crack extension occurred (as indicated in Figs. 8B–C) as the fracture mechanism changed to cleavage or mixed modes. The ductile to brittle transition appears to occur close to −45°C, with the impact toughness and final displacement decreased. The dominance of brittle fracture and resulting low impact toughness at this transition temperature range leads to increased scatter in toughness (i.e., FZ toughness in cold-wire laser weld with a WFR of 12 m/min is lower than that

of autogenous laser weld), and mostly overlapping toughness values for the varying weld metals at low temperatures of −20°C and −45°C, as shown in Fig. 9. Decreased influence of microstructure on weld metal toughness at low temperatures was also discussed in a previous report (Ref. 12) investigating GMAW of X80 steel. Even at −45°C, however, the absorbed energy for all the laser welds with varying parameters meet the requirement of APL 5L standard for line pipe, which indicates that the average absorbed energy of X80 pipe weld should reach 40 J for full-size test samples, and 20 J for 5-mm-thick sub-size samples at a test temperature of 0°C or, if agreed, a lower test temperature.

Figures 10 and 11 show the SEM images of the Charpy fracture surfaces of the samples tested at 0°C and −20°C, respectively. The presence of dimples confirmed that both the autogenous laser weld and the cold-wire laser weld with a WFR of 12 m/min exhibit ductile fracture at 0°C, as shown in Fig. 10. At −20°C, the ductile fracture was initiated at the root of the notch, as the fracture surfaces close to the notch area exhibited dimple structure, as shown in Fig. 11A and 11c. As the crack propagated towards the middle area, unstable crack extension occurred as the fracture mechanism changed to cleavage mode, which was confirmed by the quasi-cleavage feature of the fracture surfaces shown in Figs. 11B and 11D. This kind of fracture appearance is typical for Charpy tests in
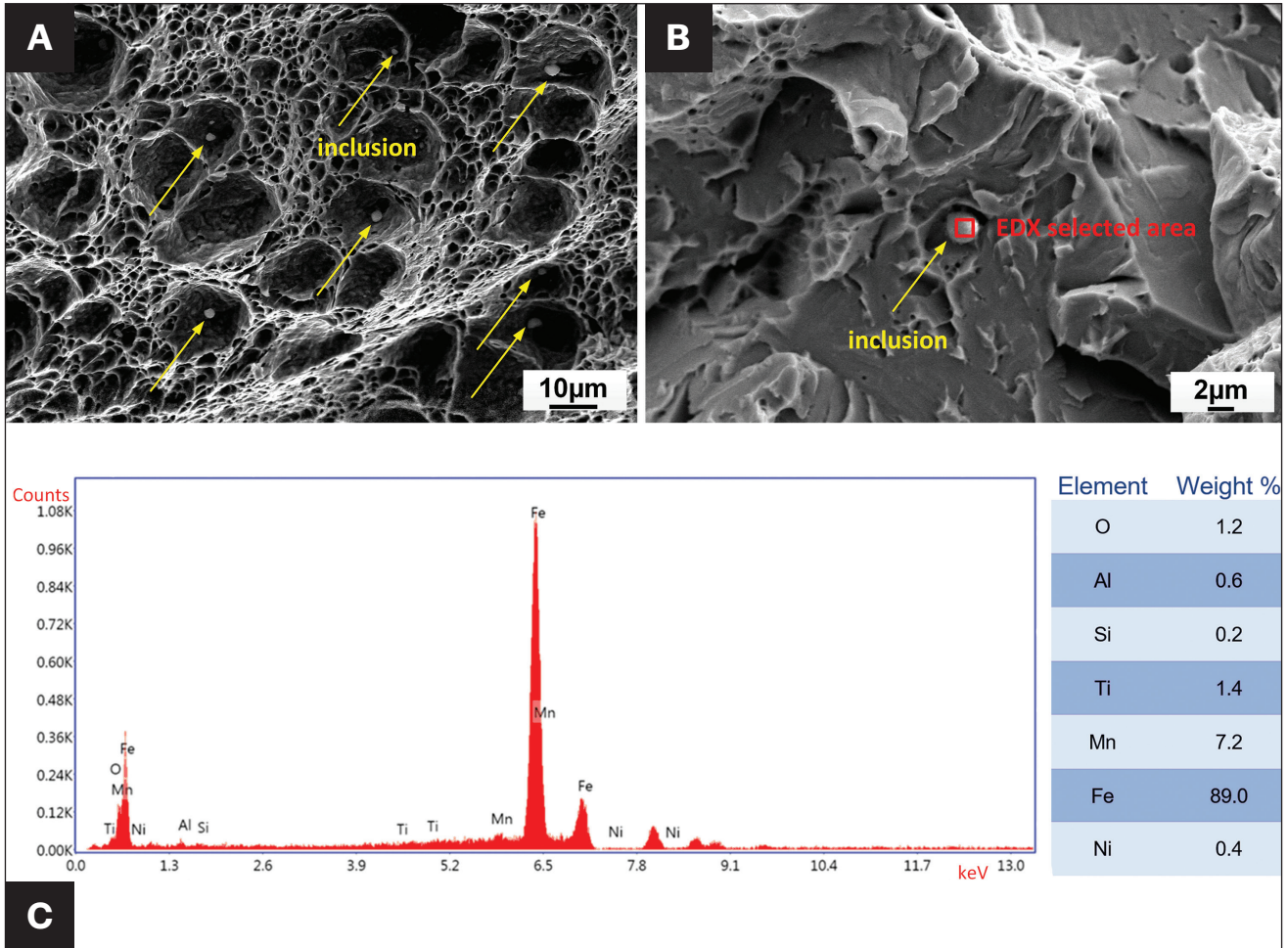
Fig. 12 — A — SEM image of Charpy fracture surface showing the presence of inclusions in the weld metal of cold-wire laser weld with a WFR of 12 m/min, tested at 0°C; B — SEM image of Charpy fracture surface showing the EDX scanning area and the presence of inclusion in the weld metal of cold-wire laser weld with a WFR of 12 m/min, tested at −20°C; C — EDX spectrum and chemical composition of the inclusion.

the transition-temperature range, according to ASTM E23. Similar Charpy fracture appearances in X80 steel at low testing temperatures were also found in a previous report (Ref. 13), with the observation close to the notch showing a small ductile layer associated with the crack initiating stage, and the remaining part being cleavage. The SEM fractography also revealed the presence of inclusions in the weld metal of cold-wire laser weld with a WFR of 12 m/min, as shown in Figs. 12A–B. EDX results (in Fig. 12C) indicated that the inclusions were mainly manganese, titanium and oxygen-based, and most likely corresponded to Mn and Ti-based oxide inclusions, which were reported to be effective nucleation sites for AF in carbon steels (Refs. 12, 14, 15), and thus explains the formation of acicular ferrite in the weld metal of cold/hot-wire laser weld.

Conclusions

The findings presented reveal the influences of filler material volume and wire preheat on the microstructure and mechanical properties in X80 steel laser root welds. In particular:

1. The addition of ER70S-6 filler wire reduced the hardness of the upper region of FZ but had limited effect on the bottom root of the fusion zone, which was due to the uneven distribution of the filler material and the resulting inhomogeneous microstructure. The hardness of the upper region of the FZ in the autogenous laser weld was around 26 HV higher than that in the hot-wire laser weld with a WFR of 12 m/min, due to the presence of more bainite.

2. Fracture occurred at base metal during the tensile tests, which indicated that weld metal strength overmatch was achieved with the welding parameters tested. Bainite and acicular ferrite generated in the weld metal provided a strength higher than that of the base metal.

3. Up to a 26% increase in Charpy impact toughness of the weld metal was achieved at 0°C with wire feed. The presence of acicular ferrite with an interlocking structure formed by wire addition accounts for the improved crack arrest ability of the weld metal. The ductile to brittle transition occurred

as the temperature decreased to –20°C and –45°C, leading to lower weld metal toughness.

Acknowledgments

References

1. Yang, H., Chen, J., Huda, N., and Gerlich, A. P. 2022. Effect of beam wobbling on microstructure and hardness during laser welding of X70 pipeline steel. *Science and Technology of Welding and Joining* 27(5): 326–338. DOI: 10.1080/13621718.2022.2053395

2. Salminen, A. 2010. The filler wire – Laser beam interaction during laser welding with low alloyed steel filler wire. *Mechanika* 84(4): 67–74. DOI: 10.5755/j01.mech.84.4.15914

3. Lehner, C., Reinhart, G., and Schaller, L. 1999. Welding of die-casted magnesium alloys for production. *Journal of Laser Applications* 11(5): 206–210. DOI: 10.2351/1.521865

4. Lampa, C. 1995. Practical and theoretical aspects of laser welding. Ph.D. dissertation. Norrbotten County, Luleå University of Technology.

5. Phillips, R. H., and Metzbower, E. A. 1992. Laser beam welding of HY80 and HY100 steels using hot welding wire addition. *Welding Journal* 71: 201-s.

6. Steen, W. M. 1980. Arc augmented laser processing of materials. *Journal of Applied Physics* 51(11): 5636-5641. DOI: 10.1063/1.327560

7. Zhenglong, L., Caiwang, T., Yanbin, C., and Zhongshao, S. 2013. Microstructure and mechanical properties of fiber laser-metal active gas hybrid weld of X80 pipeline steel. *Journal of Pressure Vessel Technology* 135(1). DOI:10.1115/1.4006347

8. Näsström, J., Frostevarg, J., and Kaplan, A. F. H. 2017. Multipass laser hot-wire welding: Morphology and process robustness. *Journal of Laser Applications* 29(2): 022014. DOI: 10.2351/1.4983758

9. Wei, H., Zhang, Y., Tan, L., and Zhong, Z. 2015. Energy efficiency evaluation of hot-wire laser welding based on process characteristic and power consumption. *Journal of Cleaner Production* 87: 255–262. DOI: 10.1016/j.jclepro.2014.10.009

10. Metzbower, E. A., Bhadeshia, H. K. D. H., and Phillips, R. H. 1994. Microstructures in hot wire laser beam welding of HY 80 steel. *Materials Science and Technology* 10(1): 56–59. DOI: 10.1179/mst.1994.10.1.56

11. Yang, H., Chen, J., Huda, N., Zhao, X., and Gerlich, A. P. 2023. Effect of wire preheat and feed rate in X80 steel laser root welds: Part 1 – Microstructure. *Welding Journal*: *107s-118s. DOI: 10.29391/2024.103.010*

12. Midawi, A. R. H., Santos, E. B. F., Huda, N., Sinha, A. K., Lazor, R., and Gerlich, A. P. 2015. Microstructures and mechanical properties in two X80 weld metals produced using similar heat input. *Journal of Materials Processing Technology* 226: 272–279. DOI: 10.1016/j.jmatprotec.2015.07.019

13. Huda, N., Midawi, A., Gianetto, J. A., and Gerlich, A. P. 2021. Continuous cooling transformation behaviour and toughness of heat-affected zones in an X80 line pipe steel. *Journal of Materials Research and Technology* 12: 613–628. DOI: 10.1016/j.jmrt.2020.11.011

14. Prokić-Cvetković, R. M., Milosavljević, A. J., Sedmak, A. S., Popović, O. D., and Petronić, S. J. 2006. Formation of acicular ferrite on non-metallic inclusion in low-alloy welded joints. *Proceedings of 10th International Research/Expert Conference 'Trends in the Development of Machinery and Associated Technology':* 1315–1318. Barcelona, Spain.

15. Beidokhti, B., Koukabi, A. H., and Dolati, A. 2009. Influences of titanium and manganese on high strength low alloy SAW weld metal properties. *Materials Characterization* 60(3): 225–233. DOI: 10.1016/j.matchar.2008.09.005

HANWEN YANG (*h376yang@uwaterloo.ca*), **NAZMUL HUDA**, **XIAOYE ZHAO**, and **ADRIAN P GERLICH** are with the Centre for Advanced Materials Joining (CAMJ), Department of Mechanical and Mechatronic Engineering, University of Waterloo, Waterloo, Ontario, Canada. **JAMES CHEN** is with CanmetMATERIALS, Natural Resources Canada, Hamilton, Ontario, Canada.